

# Improved Fourier Analysis of Periodically Patterned Graphene Sheets Embedded in Multilayered Structures and Its Application to the Design of a Broadband Tunable Wide-Angle Polarizer

Hoda Fadakar, *Student Member, IEEE*, Amir Borji, *Member, IEEE*,  
Abolghasem Zeidaabadi Nezhad, *Member, IEEE*, and  
Mahmoud Shahabadi, *Senior Member, IEEE*

**Abstract**—Numerical modeling of periodically patterned graphene sheets (PPGS) embedded in planar multilayered media using Fourier-based methods suffers from very slow convergence because of the fact that the conductivity is zero in unfilled areas of the patterned surface and, thus, the so-called Li's inverse rule is not applicable. In this paper, a simple and efficient approach is proposed to overcome this problem such that the exact boundary condition can be applied and the surface current density on PPGS can be obtained accurately. Here, the PPGS is modeled as a conductive surface and only its conductivity representation by the Fourier series is modified. The proposed method can be used easily for 1-D and 2-D periodic structures without the need to change the basic formulations of Fourier-based methods. Fast convergence and accuracy of the method will be demonstrated by computing the absorption of 1-D and 2-D PPGS. Moreover, the proposed method is utilized to design a wideband tunable wide-angle polarizer consisting of two-parallel PPGS separated by a  $0.5\text{-}\mu\text{m}$  layer of  $\text{SiO}_2$ . The transmittance of the structure exceeds 95% from microwaves up to 2 THz.

**Index Terms**—Periodically patterned graphene sheets, Fourier-based methods, fast convergence, broadband and wide-angle polarizer.

## I. INTRODUCTION

GRAPHENE, made of a two dimensional lattice of carbon atoms, is an attractive material due to its unique properties and there has been a huge interest in its photonic and electronic applications in recent years [1]–[4]. It has been shown that in terahertz and mid-infrared frequencies the imaginary part of the graphene conductivity can be negative. Thus, it can support ultra-confined surface plasmon polariton waves [5]–[9]. Moreover, the possibility of having

periodically patterned graphene sheets (PPGS) embedded in multilayered media has been exploited to design numerous plasmonic devices such as notch filters, terahertz linear polarizers [10]–[12], and terahertz absorbers [13]–[16]. Hence, having a fast convergent method for numerical analysis of such structures has become a prime focus of research recently [17]–[19].

Fourier-based methods such as Fourier Modal Method (FMM), which is also known as rigorous coupled-wave analysis (RCWA) [20], and Transmission-Line Formulation (TLF) [21], [22] are the most common methods for modeling grating structures. Applying Li's inverse rule [23] enables these methods to appropriately model almost all grating structures in optical frequencies. Using these Fourier-based methods, the PPGS can be modeled as a dielectric layer of nonzero but very small thickness of  $h$  and with an effective dielectric constant of  $\epsilon_r = 1 - i\sigma_g/h\omega\epsilon_0$  where  $\sigma_g$  is the surface conductivity of graphene [7], [13]. We will call this approach “*nonzero thickness modeling*” throughout this paper. By computing the eigenvalues and eigenvectors of the resulting periodic boundary value problem, the reflection, transmission, and absorption characteristics of PPGS can be obtained. However, the computational time increases dramatically for 2D PPGS by increasing the number of Floquet harmonics.

An alternative procedure is to model PPGS as a conductive surface in the boundary between the two regions where it is deposited. There is a great deal of research on conducting interfaces [24]–[26]. In this way there is no need to solve an eigenvalue problem for the PPGS, thus it is more efficient in terms of computation time. However, because the surface conductivity is zero in unfilled areas of the unit cell, Li's inverse rule [23] cannot be applied and convergence of this procedure is very poor. Recently, an approximate boundary condition has been proposed in [17] and [18] which makes it possible to use Li's inverse rule and improve the convergence. In this approach, it is assumed that the transverse electric field is constant in a boundary region with a fictitious height. The height chosen for this artificial boundary layer has a profound effect on the rate of convergence.

In this paper, we propose a new approach to model PPGS as a conductive surface and to use Li's inverse rule such

Manuscript received January 1, 2017; revised March 2, 2017; accepted March 23, 2017. Date of publication April 24, 2017; date of current version May 3, 2017. (*Corresponding author: Hoda Fadakar.*)

H. Fadakar and A. Zeidaabadi Nezhad are with the Department of Electrical and Computer Engineering, Isfahan University of Technology, Isfahan 84156-83111, Iran (e-mail: hoda.fadakar@gmail.com).

A. Borji is with the Department of Electrical and Computer Engineering, University of Waterloo, Waterloo, ON N2L 3G1, Canada, and also with the Department of Electrical Engineering, Sharif University of Technology, Tehran 14588-89694, Iran.

M. Shahabadi is with the Center of Excellence on Applied Electromagnetic Systems, School of Electrical and Computer Engineering, University of Tehran, Tehran 1439957131, Iran.

Color versions of one or more of the figures in this paper are available online at <http://ieeexplore.ieee.org>.

Digital Object Identifier 10.1109/JQE.2017.2696496

that the exact boundary conditions can be applied. It will be shown that implementation of the proposed approach for 1D and 2D PPGS is very straightforward and there is no need to change the basic formulations and boundary conditions of TLF or any other Fourier-based method that is adopted for numerical analysis. This approach in comparison with nonzero thickness modeling and Laurent's rule has higher accuracy and its computation time is much less than that of nonzero thickness modeling since there is no need to solve an eigenvalue problem for the PPGS, specially for 2D PPGS. The effectiveness of the proposed approach is demonstrated by recomputing the previously obtained results and by using Ansys HFSS.

Finally, using the proposed method, a broadband polarizer consisting of two PPGS deposited on both sides of a thin SiO<sub>2</sub> layer is designed. The compact polarizer maintains high performance, with TM transmittance larger than 95% and extinction ratio exceeding 10dB, from microwaves up to 2THz and with incident angles up to 90°. Furthermore, owing to the graphene properties, the bandwidth can be adjusted with variation of the Fermi energy or, equivalently, the applied electrostatic bias.

## II. FORMULATION

Here the TLF which is a variant of the FMM is used to analyze multilayered structures that contain 1D or 2D PPGS [21], [22]. In this formulation, the transverse electric and magnetic field components,  $[E_{xi}, E_{yi}]$  and  $[H_{yi}, -H_{xi}]$ , are considered as transmission line voltages and currents, respectively, and they are represented by Fourier series expansions in each layer. Each Fourier mode represents a separate transmission line with its own propagation constant. These parallel transmission lines are coupled through inhomogeneous layers such as gratings or patterned sheets within the structure. Finally, the necessary boundary conditions, namely, the continuity of line voltages and currents on the boundaries, are enforced. Knowing the incident wave, field components in all layers including the transmitted and reflected waves at the bottom and top of the structure can be calculated.

### A. Modeling the Periodically Patterned Graphene Sheet in TLF

A two-layer planar structure which contains a 1D and a 2D PPGS is shown in Fig. 1(a) and (b). PPGS has a surface conductivity function defined by  $\sigma_s(x, y)$  which is equal to the surface conductivity of graphene,  $\sigma_g$ , where the graphene exists and is zero elsewhere. The carrier concentration in PPGS is controlled by using an ion-gel top gate, which allows a large variation of the Fermi energy level through electrostatic gating [27], [28]. The top and side view of a typical gated structure is shown in Fig. 1(c). A top gate metallic contact can be fabricated on the ion-gel layer.

Typically, the nonzero thickness model which was described in *Introduction* is employed to model the PPGS. However, this procedure is very time consuming specially for 2D PPGS because of extremely large matrices that are involved [13]. Another approach is to model the graphene sheet on the

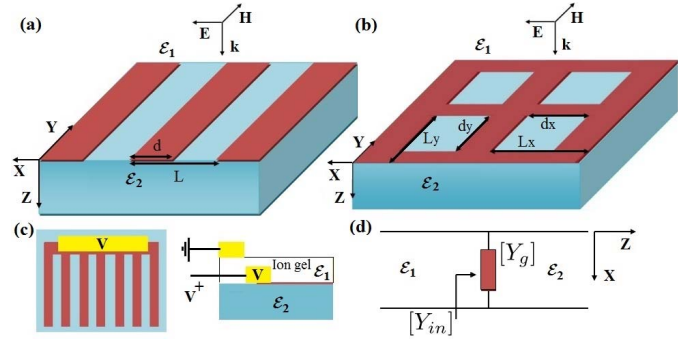


Fig. 1. A planar two-layer structure containing (a) 1D ribbons of graphene with period  $L$  and width  $d$  (b) a 2D periodic rectangular lattice of graphene holes with periods  $L_x$  and  $L_y$  in the  $x$  and  $y$  directions, respectively. The size of each window is  $d_x \times d_y$ . Permittivities of the two half-spaces above and below the PPGS are  $\epsilon_1$  and  $\epsilon_2$ . (c) Top and side view of a gated structure. (d) Equivalent circuit model of the two-layer structure containing a PPGS.

boundary between two layers as a current sheet whose surface current density  $\vec{J}_s$  is related to the tangential electric field by the Ohm's law:  $\vec{J}_s = \sigma_s \vec{E}_{\text{tan}}$ . In TLF the graphene sheet enters the formulation as a shunt admittance as shown in Fig. 1(d). In the case of 2D PPGS the admittance matrix representing the graphene sheet is  $[Y_g]$  given by:

$$[Y_g] = \begin{bmatrix} [[\sigma_s]] & \mathbf{0} \\ \mathbf{0} & [[\sigma_s]] \end{bmatrix} \quad (1)$$

where  $[[\sigma_s]]$  is a matrix containing the Fourier expansion coefficients,  $\sigma_{m,n}$ , of the surface conductivity function  $\sigma_s(x, y)$  with respect to the  $x$  and  $y$  coordinates.

In the case of 1D PPGS (graphene ribbons), TM<sup>z</sup> and TE<sup>z</sup> polarizations are decoupled. If the structure is periodic along the  $x$ -axis and is uniform along  $y$  ( $\partial/\partial y = 0$ ) then, the TM<sup>z</sup> polarization contains  $E_z$ ,  $E_x$ , and  $H_y$  only. Therefore,  $[E_{xi}(z)]$  and  $[H_{yi}(z)]$  represent, respectively, the voltages and currents of the equivalent transmission line network and the admittance matrix  $[Y_g]$  is defined by:

$$[Y_g] = [\sigma_s] \quad (2)$$

where  $[\sigma_s]$  is a matrix containing Fourier expansion coefficients of the surface conductivity function  $\sigma_s(x)$  with respect to the  $x$ . Having  $[Y_g]$  as shown in Fig. 1(d) between the two media, the input admittance  $[Y_{in}]$ , seen at the top of the graphene sheet, is given by:

$$[Y_{in}] = [Y_{c2}] + [Y_g] \quad (3)$$

where  $[Y_{c2}]$  is the characteristic admittance matrix of the substrate layer which is assumed to be semi-infinite here. The characteristic admittance matrix of each layer which is defined as complex current amplitude of upward wave divided by its complex voltage amplitude, is given by:

$$[Y_{ci}] = [Q^i][P^i]^{-1} \quad (4)$$

Here,  $[P^i]$  and  $[Q^i]$  are matrices which contain eigenvectors of voltages and currents respectively [21]. Knowing the incident voltage wave  $[V_1^+(z=0)]$  and applying the continuity of line voltages at the interface,  $[V_2(z=0)] = [V_1(z=0)] \triangleq$

$[V(z=0)]$ , the reflected and transmitted voltage waves are obtained as follows:

$$([Y_{c1}] + [Y_{in}])[V_1^-(z=0)] = ([Y_{c1}] - [Y_{in}])[V_1^+(z=0)] \quad (5)$$

$$[V_2(z=0)] = [V_2^+(z=0)] = [V_1^+(z=0)] + [V_1^-(z=0)] \quad (6)$$

Similarly, the total currents on the left and right side of  $[Y_g]$  in Fig. 1(d) are given by:

$$[I_1(z=0)] = [Y_{c1}] ([V_1^+(z=0)] - [V_1^-(z=0)]) \quad (7)$$

$$[I_2(z=0)] = [I_2^+(z=0)] = [Y_{c2}][V(z=0)] \quad (8)$$

It can be shown that (5) contains a term that equals the current density on the graphene sheet which, according to the Ohm's law, is given by:

$$\vec{J}_s = [Y_g] ([V_1^+(z=0)] + [V_1^-(z=0)]) \quad (9)$$

The surface current density normal to the edges of graphene ribbons must be zero, *i.e.* it must be a continuous function [17]. However, the Laurent's rule cannot preserve its continuity uniformly because it is a product of two discontinuous functions and this leads to poor convergence of computations. Moreover, because  $\sigma_s(x, y)$  is zero where the graphene does not exist, applying Li's inverse rule is impossible [23].

### B. Proposed Approach

In order to be able to use Li's inverse rule, the surface conductivity must be nonzero everywhere. If we write:

$$\sigma_s(x, y) = (\sigma_s(x, y) + \sigma_0) - \sigma_0 \quad (10)$$

in which  $\sigma_0$  is a small arbitrary constant value, then the total surface current will have two components associated with the two terms in (10) and the total surface admittance matrix,  $[Y_g]$  in Fig. 1(d) can be written as a sum of two admittance matrices. In the case of 1D PPGS we can write:

$$[Y_g] = \left[ \frac{1}{\sigma_s} \right]^{-1} \approx \left[ \frac{1}{\sigma_s + \sigma_0} \right]^{-1} + [-\sigma_0] \triangleq [\tilde{Y}_g] \quad (11)$$

where  $\left[ \frac{1}{\sigma_s + \sigma_0} \right]$  is a square matrix that contains the Fourier series coefficients of  $1/(\sigma_s(x, y) + \sigma_0)$  and  $[-\sigma_0]$  is a diagonal matrix having  $-\sigma_0$  on its diagonal elements.  $[\tilde{Y}_g]$  is the new admittance matrix which is a close approximation of the original one if  $\sigma_0$  and the truncation order of Fourier series are chosen properly. Note that the "approximate" sign in (11) is due to the truncation of infinite Fourier series. If all terms could be retained, the two sides in (11) would be mathematically equal. By using this decomposition of surface conductivity, the total surface current will have two components:

$$\vec{J}_s = \vec{J}_{s1} + \vec{J}_{s2} = \left[ \frac{1}{\sigma_s + \sigma_0} \right]^{-1} [V(z=0)] + [-\sigma_0][V(z=0)] \quad (12)$$

Note that  $[V(z=0)]$  represents the total tangential electric field at  $z=0$ . Similarly, in the case of 2D PPGS,

the admittance matrix  $[Y_g]$  is approximately decomposed into two terms:

$$[\tilde{Y}_g] = \begin{bmatrix} \left[ \frac{1}{\sigma_s + \sigma_0} \right] & \mathbf{0} \\ \mathbf{0} & \left[ \frac{1}{\sigma_s + \sigma_0} \right] \end{bmatrix}^{-1} + [-\sigma_0] \quad (13)$$

The sub-matrices  $\left[ \frac{1}{\sigma_s + \sigma_0} \right]$  ( $\left[ \frac{1}{\sigma_s + \sigma_0} \right]$ ) are computed by applying the Li's inverse rule with respect to the  $x$  ( $y$ ) and then applying the Laurent's rule in the  $y$  ( $x$ ) direction [29]. Since  $J_x(x, y)$  is only continuous in the  $x$  direction, it is sufficient to apply Li's inverse rule with respect to the  $x$  and the Laurent's rule with respect to the  $y$ . Similarly, in computing  $J_y(x, y)$  it is sufficient to apply Li's inverse rule with respect to the  $y$  and then the Laurent's rule with respect to the  $x$ .

After careful examination of numerous examples we found that the optimum value for  $\sigma_0$  is equal to the effective surface conductivity of the two neighboring media in the absence of graphene sheet which is defined by:

$$\sigma_0 = i\omega\epsilon_0\Delta \left( \frac{\epsilon_{r1} + \epsilon_{r2}}{2} \right) \triangleq \sigma_{0,\text{eff}} \quad (14)$$

$\Delta$  is an arbitrary parameter with physical dimension of length but it is not a fictitious thickness.  $\epsilon_{r1}$  and  $\epsilon_{r2}$  are complex dielectric constants of the two neighboring media. This effective surface conductivity can be derived by applying the Ampère's law at the boundary between the two media [18]. Convergence of (12) is closely related to the value of  $\sigma_0$ . By increasing  $\Delta$  the convergence rate of  $J_{s1}$  increases while, on the other hand, the approximation in (11) is more accurate for smaller  $\Delta$ . Thus, there is a tradeoff in choosing  $\Delta$ . However, this method is convergent for a wide range of  $\Delta$ . Different value of  $\Delta$  only will affect the convergence rate. In general,  $\sigma_0$  is a complex number with positive real part. Numerical examples showed that by choosing  $\Delta$  as the minimum of  $\{L_x/100, L_y/100, d_x/5, d_y/5, (L_x - d_x)/5, (L_y - d_y)/5\}$  accurate and fast convergent results are usually achieved. However, the proposed method also shows convergent behavior for  $\sigma_0 \neq \sigma_{0,\text{eff}}$ , e.g., purely real, purely imaginary or complex values with positive and negative real and imaginary part. Only if  $\sigma_0 = -\sigma_{0,\text{eff}}$  the method fails to converge. Eq. (14) is the effective surface conductivity of neighboring media. This will be explained in the examples of the next section.

It is worth mentioning that the proposed approach can be also implemented for an anisotropic surface conductivity of magnetically biased graphene and for the bio-sensing applications in the ultraviolet range where interband  $\pi$  plasmons are observed around 250 nm wavelength [30], [31].

### III. ANALYSIS OF 1D PPGS

To verify the proposed method, the example given in [14] is revisited. The structure is shown in Fig. 1(a). It consists of an array of graphene ribbons with a period of  $L = 8\mu\text{m}$  and a width of  $d = 4\mu\text{m}$  placed between two semi-infinite layers with relative permittivities of  $\epsilon_{r1} = 3$  and  $\epsilon_{r2} = 4$ . The surface conductivity of graphene ribbons is obtained, within

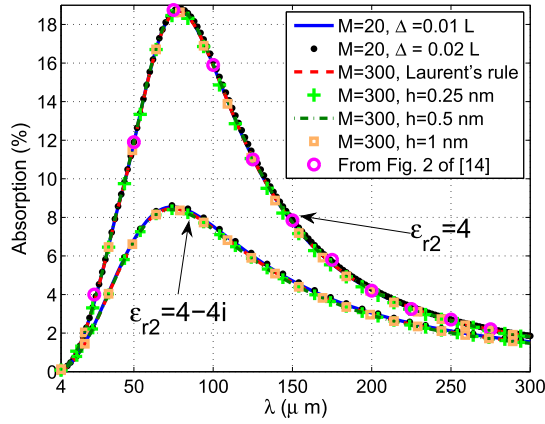


Fig. 2. Absorption of 1D PPGS as a function of free-space wavelength. The period and width of ribbons are  $L = 8\mu\text{m}$  and  $d = 4\mu\text{m}$ , respectively. Dielectric constant of the top half space is  $\epsilon_{r1} = 3$

the random-phase approximation [32], from:

$$\sigma_g = \frac{ie^2 E_F}{\pi \hbar^2 (i2\pi \tau^{-1} - \omega)} + \frac{e^2}{4\hbar} \left[ H(\hbar\omega - 2E_F) - \frac{i}{\pi} \ln \left| \frac{\hbar\omega - 2E_F}{\hbar\omega + 2E_F} \right| \right] \quad (15)$$

where  $e$  is the electron charge,  $E_F$  is the Fermi energy,  $\hbar$  is the Planck constant,  $\tau$  is the relaxation time and  $H$  is the Heaviside step function [15]. Here, the Fermi energy and relaxation time are  $E_F = 0.6\text{eV}$  and  $\tau = 0.25\text{ps}$ , respectively.

A TM polarized plane wave illuminates the structure normally from the top as shown in Fig.1(a). The absorption of the graphene ribbons was computed as a function of free-space wavelength using the proposed approach with truncation order of  $M = 20$  and  $\Delta = 0.01L, 0.02L$ . The results are shown in Fig.2. The computed absorption is compared with that obtained in [14] and also with those calculated by nonzero thickness modeling of graphene ribbons with truncation order of  $M = 300$  and thicknesses of  $h = 0.25\text{nm}$ ,  $h = 0.5\text{nm}$ ,  $h = 1\text{nm}$ , and with the results of Laurent's rule that uses (2) in (9) with truncation order of  $M = 300$ . It is seen that the results are in very good agreement; however, we should bear in mind that the proposed approach merely needs a truncation order of  $M = 20$  to converge. The total CPU time required to calculate and plot 149 data points in Fig.2 is 5.2sec for our proposed method, 5635sec for nonzero thickness model, and 72sec for employing the Laurent's rule.

The real part of total surface current density  $\vec{J}_s$  on the PPGS computed with a truncation order of  $M = 20$  at  $\lambda = 200\mu\text{m}$  is shown in Fig.3. Note that for TM polarization, the surface current density only has  $\hat{x}$  component transverse to the graphene ribbons. The real parts of  $\vec{J}_{s1}$  and  $\vec{J}_{s2}$ , defined in (12), are also plotted in the same figure. It is seen that by using the proposed approach continuity of surface current density is preserved to a high degree of accuracy. It is worth mentioning that if a smaller  $\Delta$  is selected, the current density becomes more uniform in the neighborhood of the edge of each graphene ribbon. However, a very small  $\Delta$  causes slow convergence for  $\vec{J}_{s1}$ . To demonstrate this effect, the real part

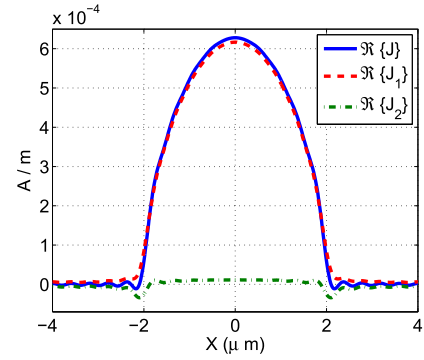


Fig. 3. Real parts of the total current  $\vec{J}_s$  (solid line),  $\vec{J}_{s1}$  (dashed line), and  $\vec{J}_{s2}$  (dash-dotted line) on the PPGS in one unit cell computed with  $M = 20$  and  $\Delta = 0.01L$  at  $\lambda = 200\mu\text{m}$ .  $\epsilon_{r2} = 4$  and other parameters are the same as Fig.2.

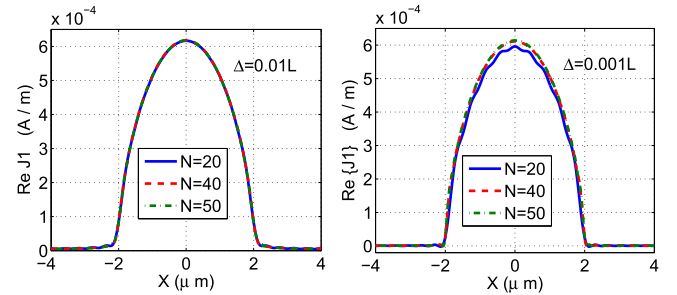


Fig. 4. Real part of  $\vec{J}_{s1}$  on PPGS in one unit cell computed by different truncation orders for  $\Delta = 0.01L$  and  $\Delta = 0.001L$  at  $\lambda = 200\mu\text{m}$ .  $\epsilon_{r2} = 4$  and other parameters are the same as Fig.2.

of  $\vec{J}_{s1}$  for  $\Delta = 0.01L$  and  $\Delta = 0.001L$  are plotted in Fig.4. These results show that, for  $\Delta = 0.01L$ , a truncation order of 20 is sufficient to achieve convergent results while for  $\Delta = 0.001L$  the truncation order must be at least 40. In fact, a smaller value for  $\Delta$  leads to a larger condition number for  $[Y_g]$  matrix in (11).

We also consider the structure in Fig.1(a) with previous parameters but with  $\epsilon_2 = (4 - 4i)\epsilon_0$ . Absorption of graphene ribbons, excluding the absorption by the substrate, with truncation order of  $M = 20$ ,  $\Delta = 0.01L$  and  $\Delta = 0.02L$  are also shown in Fig.2. The results are compared with those of the Laurent's rule and nonzero thickness modeling of graphene sheet with truncation order of  $M = 300$  and thicknesses of  $h = 0.25\text{nm}$ ,  $h = 0.5\text{nm}$ ,  $h = 1\text{nm}$ . It is clear that the proposed approach is very accurate and highly convergent. Note that the nonzero thickness modeling requires a matrix of size  $601 \times 601$  to be diagonalized which significantly increases the computation time.

The relative errors in computation of absorption with  $\epsilon_{r2} = 4 - 4i$  at  $\lambda = 100\mu\text{m}$  are shown in Fig.5 as a function of truncation order for various methods. The result of the proposed method for a truncation order of  $M = 500$  was taken as reference. At this truncation order, Laurent's rule, nonzero thickness method, and the proposed method with  $\Delta = 0.01L$  converge to identical values down to three decimal digits. Convergence rates of the Laurent's rule, the nonzero thickness model, the proposed approach with different  $\Delta$  val-

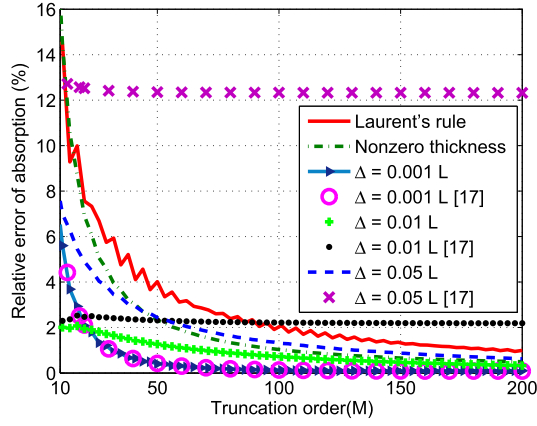


Fig. 5. Relative errors in computation of absorption curves shown in Fig. 2 with  $\varepsilon_{r2} = 4 - 4i$  at  $\lambda = 100\mu\text{m}$  vs. truncation order.

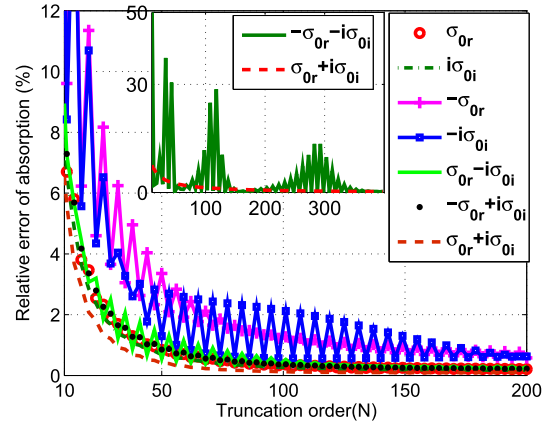


Fig. 7. Relative errors in computation of absorption of ribbons on  $\varepsilon_{r2} = 4 - 4i$  at  $\lambda = 100\mu\text{m}$  vs. truncation order for various  $\sigma_0$  value.

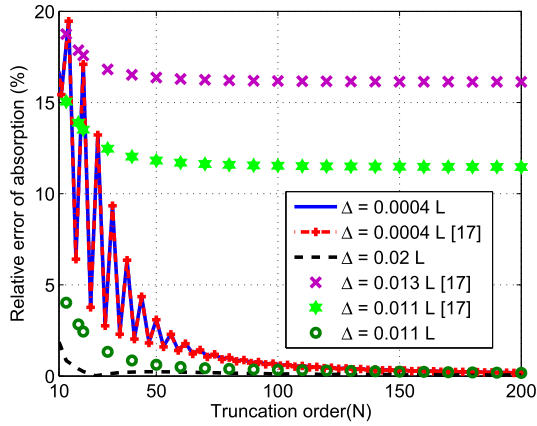


Fig. 6. Relative errors in computation of absorption curves shown in Fig. 2 with  $\varepsilon_{r2} = 4 - 4i$  at  $\lambda = 9\mu\text{m}$  vs. truncation order.

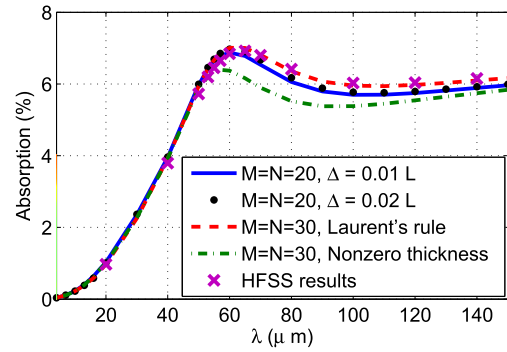


Fig. 8. Absorption of 2D periodic square array of graphene holes as a function of free-space wavelength. The period of square array is  $L_x = L_y = 8\mu\text{m}$  and the width of each graphene hole is  $d_x = d_y = 6.4\mu\text{m}$ . The dielectric constants of the two half-spaces above and below the graphene surface are  $\varepsilon_{r1} = 3$  and  $\varepsilon_{r2} = 4$ .

ues, and those of using [17] are all illustrated in this figure. The new method shows a superior performance specially at small truncation orders. Here, the optimum value of  $\Delta$  for the proposed approach and that of [17] is  $\Delta = 0.001L$ . In Fig. 6, the relative errors in computation of absorption with  $\varepsilon_{r2} = 4 - 4i$  at  $\lambda = 9\mu\text{m}$  are shown as a function of truncation order for various methods. The optimum value of  $\Delta$  using the proposed approach is  $\Delta = 0.02L$  while for the method described in [17] is  $\Delta = 0.0004L$ .

In Fig. 7, the relative errors in computation of absorption with  $\varepsilon_{r2} = 4 - 4i$  at  $\lambda = 100\mu\text{m}$  are shown as a function of truncation order for various  $\sigma_0$  value. According to (14) for  $\Delta = L/1000$  the value of  $\sigma_{0,\text{eff}} = \sigma_{0r} + i\sigma_{0i}$  is  $2.67 \times 10^{-6} + i4.67 \times 10^{-6}$ . The convergence rate for different sign of real part and imaginary part and also for purely real and purely imaginary values of  $\sigma_0$  are shown in this figure. It is seen that the proposed method shows convergence for all these values. However, only for inverted sign of  $\sigma_0 = -\sigma_{0r} - i\sigma_{0i}$  this method does not converge. To illustrate this, the relative errors in computation of absorption for  $\Delta = 0.05L$ ,  $\sigma_0 = -\sigma_{0r} - i\sigma_{0i} = -1.33 \times 10^{-4} - i2.33 \times 10^{-4}$  and for  $\sigma_0 = \sigma_{0r} + i\sigma_{0i}$  are shown in the inset of Fig. 7. When the neighboring media are lossless  $\sigma_{0,\text{eff}}$  is purely imaginary. Hence, only purely

imaginary value of  $\sigma_0 = -\sigma_{0,\text{eff}}$  will not converge and other different values of  $\sigma_0$  e.g. purely real, complex with arbitrary sign of real and imaginary part will have convergent behaviors.

#### IV. ANALYSIS OF 2D PPGS

In this section a two-dimensional array of square windows in graphene with periods of  $L_x = L_y = L = 8\mu\text{m}$  and side lengths of  $d_x = d_y = 6.4\mu\text{m}$  is considered. This array is placed between two semi-infinite layers as shown in Fig. 1 b. The electric field of the incident wave is parallel to the  $x$ -axis and illuminates the structure normally from the top. We consider the lossless substrate where the relative permittivities of the top and bottom layers are  $\varepsilon_{r1} = 3$  and  $\varepsilon_{r2} = 4$ , respectively. The Fermi energy and relaxation time are  $E_F = 0.4\text{eV}$  and  $\tau = 0.25\text{ps}$ , respectively. The absorption of graphene array computed as a function of free-space wavelength using the proposed approach with truncation order of  $N = M = 20$ ,  $\Delta = 0.01L$  and  $\Delta = 0.02L$  is shown in Fig. 8. The results of Laurent's rule that uses (1) in (9) and nonzero thickness model with truncation order of  $N = M = 30$  and thickness of  $0.5\text{nm}$  are also shown. To further verify the results, the absorption obtained from simulating the structure with Ansys HFSS is also provided in Fig. 8 which is in excellent agreement with our proposed method.

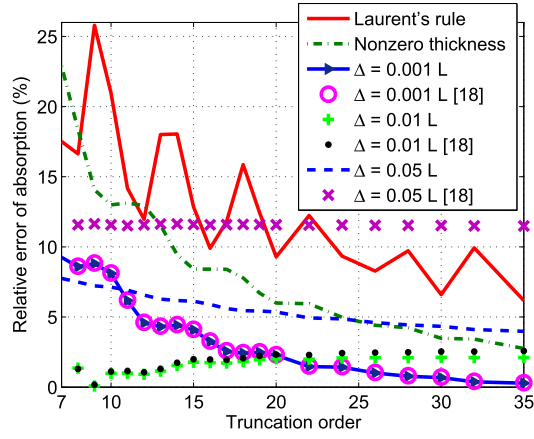


Fig. 9. Relative errors in computation of absorption curves shown in Fig. 8 at  $\lambda = 100\mu\text{m}$  as a function of truncation order.

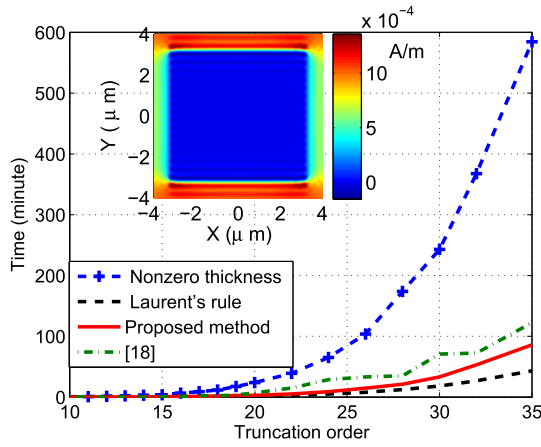


Fig. 10. The total CPU time required to calculate one data point in Fig. 8 as a function of truncation order. Real part of the  $\hat{x}$  component of the total surface current on the PPGS computed with  $N = M = 20$  and  $\Delta = 0.01L$  at  $\lambda = 100\mu\text{m}$  is shown in the inset.

To explore the convergence rate of the proposed approach, the relative errors in calculating the absorption curves in Fig. 8 at  $\lambda = 100\mu\text{m}$  as a function of truncation order are shown in Fig. 9. The result of the proposed approach with  $\Delta = 0.001L$  and truncation order of  $M = N = 40$  was taken as the reference. The results in Fig. 9 show that, similar to 1D structure, the proposed approach is convergent. The total CPU time required to calculate one data point in Fig. 8 is shown in Fig. 10. It is seen that the proposed method is much faster than nonzero thickness model. Specially, it needs a smaller truncation order for convergence. Here, the surface current density  $\vec{J}_s$  has both  $\hat{x}$  and  $\hat{y}$  components but the former is the dominant one. The real part of the  $\hat{x}$  component of total surface current computed with  $\Delta = 0.01L_x$  and  $N = M = 20$  at  $\lambda = 100\mu\text{m}$  is shown in the inset of Fig. 10. Again the proposed approach satisfies the continuity of  $J_x$  along the x-axis.

## V. BROADBAND AND WIDE ANGLE POLARIZER DESIGN

In this section, the proposed method is utilized to design and analyze a polarizer structure. The polarizer is shown

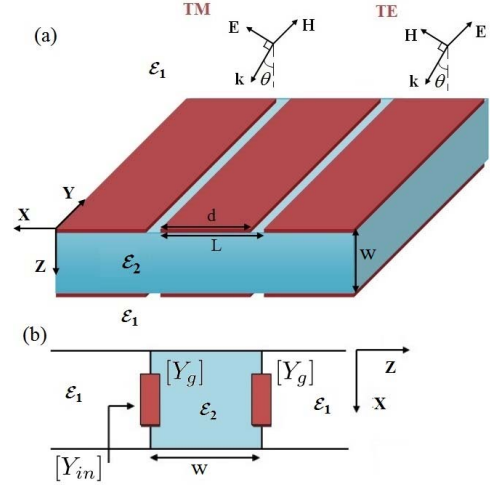


Fig. 11. (a) The proposed polarizer containing two sheets of periodically deposited ribbons of graphene on both sides of  $\text{SiO}_2$  substrate. (b) The equivalent admittance model of polarizer.

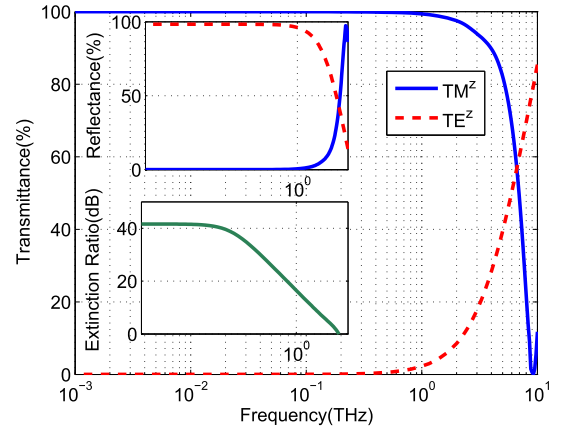


Fig. 12. Transmittance and reflectance of the polarizer vs. frequency for normal incidence. The period and width of ribbons are  $L = 1\mu\text{m}$  and  $d = 0.9\mu\text{m}$ , respectively. Extinction ratio of the polarizer at normal incidence vs. frequency is also shown in the inset.

in Fig. 11(a). It is made of two parallel arrays of graphene ribbons with the period of  $L = 1\mu\text{m}$  and width of  $d = 0.9\mu\text{m}$  deposited on both sides of  $\text{SiO}_2$  layer with a thickness of  $w = 0.5\mu\text{m}$ . The equivalent admittance model of the polarizer is shown in Fig. 11(b). The relative permittivity of  $\text{SiO}_2$  vs. wavelength is taken from [33]. The incident plane-wave illuminates the structure from the top with either  $\text{TM}^z$  (magnetic field parallel to the y-axis) or  $\text{TE}^z$  (electric field parallel to the y-axis) polarization. The parameters of graphene ribbons are:  $E_F = 1\text{eV}$  and  $\Gamma = 0.11\text{meV}$  [34], [35] or, equivalently,  $\tau = \pi/\Gamma = 18.8\text{ps}$ . The calculated transmittance/reflectance for  $\text{TM}^z$  and  $\text{TE}^z$  waves and extinction ratio at normal incidence are shown in Fig. 12. The proposed approach was utilized with truncation order of  $N = 20$  and  $\Delta = 0.01L$ . The extinction ratio (ER) is defined as  $10 \times \log_{10}(T_{\text{TM}^z}/T_{\text{TE}^z})$ , where  $T_{\text{TM}^z}$  and  $T_{\text{TE}^z}$  are the intensity transmittance of  $\text{TM}^z$  and  $\text{TE}^z$  polarized waves, respectively. Transmittance higher than 95% and extinction ratio better than 10dB are obtained over a wide band from microwaves up to 2 THz. Using

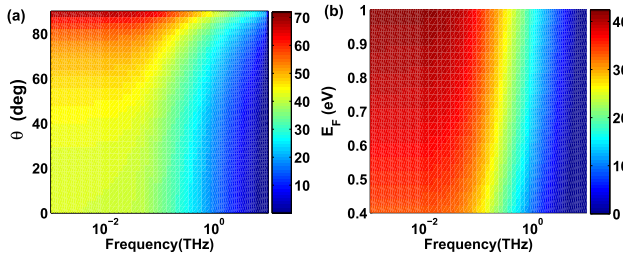


Fig. 13. Extinction ratio of the polarizer (a) as a function of frequency and incident angle (b) as a function of frequency and Fermi energy.

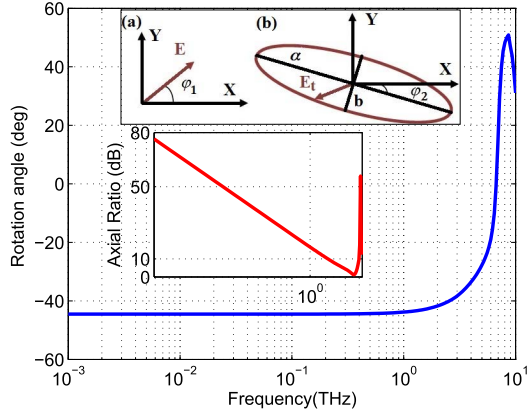


Fig. 14. The rotation angle defined by  $\phi_2 - \phi_1$  for unpolarized wave with normal incidence and with orientation of  $\phi_1 = 45^\circ$  vs. frequency. Linearly polarized incident electric field, general elliptically polarized transmitted field and axial ratio are shown in the inset.

graphene strips in contrast to the periodic arrangement of rectangular slots on a graphene sheet, which was proposed by [12] and [36], has led to a wide-band THz polarizer.

Since the reflectance of  $TE^z$  waves, shown in the inset of Fig. 12, over the same frequency band is near 98%, the designed structure can also be used as a polarization-selective beam-splitter [37], [38]. The designed polarizer also maintains its high performance at large incident angles. As shown in Fig. 13(a), the extinction ratio is actually improved with increasing the incident angle. Furthermore, the performance of the polarizer can be tuned by varying the Fermi energy  $E_F$  or, equivalently, the DC electric bias applied to the graphene ribbons. The results of extinction ratio for Fermi energies from 0.4eV to 1eV are shown in Fig. 13(b) which indicate the bandwidth of the polarizer increases.

A linearly polarized incident wave with an arbitrary orientation of the electric field vector, indicated by  $\phi_1$  in the inset of Fig. 14, can be written as sum of a TE ( $\phi_1 = 90^\circ$ ) and a TM ( $\phi_1 = 0$ ) wave. Here, the TE component of the transmitted wave is strongly attenuated while the TM one remains *almost* unchanged with its amplitude equal to  $\cos \phi_1$  times the magnitude of the electric field of incident field. This leads to the rotation of the transmitted electric field vector with respect to that of the incident wave. In general, for an arbitrary orientation of the electric field vector, the transmitted TM and TE components do not have the same phase. This phase difference results in elliptical polarization

of the transmitted wave as shown in the inset of Fig. 14. The shape and orientation of the ellipse is determined by the tilt angle  $\phi_2$  and the axial ratio which is defined as  $20 \log(a/b)$  ( $2a$  and  $2b$  are the major and minor axes of the ellipse). The rotation angle for an unpolarized wave with normal incidence and  $\phi_1 = 45^\circ$  is shown in Fig. 14. The axial ratio of the transmitted electric field is also shown in the inset. The axial ratio is larger than 10 dB and the rotation angle is almost  $-45^\circ$  up to 2 THz.

## VI. CONCLUSION

A robust and very efficient method for the analysis of periodically patterned graphene sheets embedded in layered media was presented. Here, the boundary condition applied at the surface of PPGS is exact. The proposed approach always produces convergent results regardless of the value chosen for  $\Delta$ . Moreover, the implementation of this approach is very simple and there is no need to change the basic formulation of Fourier based methods. Furthermore, since the patterned graphene sheet enters the formulation as a *surface conductivity* and Li's inverse rule is employed, the method is always highly convergent. Also because there is no need to solve an eigenvalue problem for the graphene sheet, the computation time decreases dramatically, specially for 2D structures, compared to the nonzero thickness modeling. The proposed method was used to design a wide-angle broadband tunable polarizer and to evaluate its performance. Its TM transmittance and extinction ratio exceed 95% and 10dB, respectively, in the microwave to far-infrared band.

## REFERENCES

- [1] A. R. Davoyan, V. V. Popov, and S. A. Nikitov, "Tailoring terahertz near-field enhancement via two-dimensional plasmons," *Phys. Rev. Lett.*, vol. 108, p. 127401, Mar. 2012.
- [2] M. Dragoman, A. A. Muller, D. Dragoman, F. Coccetti, and R. Plana, "Terahertz antenna based on graphene," *J. Appl. Phys.*, vol. 107, no. 10, p. 104313, 2010.
- [3] A. Vakil and N. Engheta, "Fourier optics on graphene," *Phys. Rev. B, Condens. Matter*, vol. 85, p. 075434, Feb. 2012.
- [4] M. Chen, F. Fan, L. Yang, X. Wang, and S.-J. Chang, "Tunable terahertz amplifier based on slow light edge mode in graphene plasmonic crystal," *IEEE J. Quantum Electron.*, vol. 53, no. 1, pp. 1–6, Feb. 2017.
- [5] J. T. Kim and S.-Y. Choi, "Graphene-based plasmonic waveguides for photonic integrated circuits," *Opt. Exp.*, vol. 19, no. 24, pp. 24557–24562, Nov. 2011.
- [6] G. W. Hanson, "Quasi-transverse electromagnetic modes supported by a graphene parallel-plate waveguide," *J. Appl. Phys.*, vol. 104, no. 8, p. 084314, 2008.
- [7] A. Vakil and N. Engheta, "Transformation optics using graphene," *Science*, vol. 332, no. 6035, pp. 1291–1294, 2011.
- [8] A. Y. Nikitin, F. Guinea, F. J. García-Vidal, and L. Martín-Moreno, "Edge and waveguide terahertz surface plasmon modes in graphene microribbons," *Phys. Rev. B, Condens. Matter*, vol. 84, p. 161407, Oct. 2011.
- [9] X. L. Liu, B. Zhao, and Z. M. Zhang, "Blocking-assisted infrared transmission of subwavelength metallic gratings by graphene," *J. Opt.*, vol. 17, no. 3, p. 035004, 2015.
- [10] H. Yan *et al.*, "Tunable infrared plasmonic devices using graphene/insulator stacks," *Nature Nanotechnol.*, vol. 7, no. 5, pp. 330–334, 2012.
- [11] Z. H. Zhu *et al.*, "Electrically controlling the polarizing direction of a graphene polarizer," *J. Appl. Phys.*, vol. 116, no. 10, p. 104304, 2014.
- [12] A. Fallahi and J. Perruisseau-Carrier, "Design of tunable biperiodic graphene metasurfaces," *Phys. Rev. B, Condens. Matter*, vol. 86, p. 195408, Nov. 2012.

- [13] R. Alaei, M. Farhat, C. Rockstuhl, and F. Lederer, "A perfect absorber made of a graphene micro-ribbon metamaterial," *Opt. Exp.*, vol. 20, no. 27, pp. 28017–28024, Dec. 2012.
- [14] A. Y. Nikitin, F. Guinea, F. J. García-Vidal, and L. Martín-Moreno, "Surface plasmon enhanced absorption and suppressed transmission in periodic arrays of graphene ribbons," *Phys. Rev. B, Condens. Matter*, vol. 85, p. 081405, Feb. 2012.
- [15] S. Thongrattanasiri, F. H. L. Koppens, and F. J. García de Abajo, "Complete optical absorption in periodically patterned graphene," *Phys. Rev. Lett.*, vol. 108, p. 047401, Jan. 2012.
- [16] T. R. Zhan, F. Y. Zhao, X. H. Hu, X. H. Liu, and J. Zi, "Band structure of plasmons and optical absorption enhancement in graphene on subwavelength dielectric gratings at infrared frequencies," *Phys. Rev. B, Condens. Matter*, vol. 86, no. 16, p. 165416, Oct. 2012.
- [17] A. Khavasi, "Fast convergent Fourier modal method for the analysis of periodic arrays of graphene ribbons," *Opt. Lett.*, vol. 38, no. 16, pp. 3009–3012, 2013.
- [18] S. A. H. Nekuee, A. Khavasi, and M. Akbari, "Fourier modal method formulation for fast analysis of two-dimensional periodic arrays of graphene," *J. Opt. Soc. Amer. B, Opt. Phys.*, vol. 31, no. 5, pp. 987–993, 2014.
- [19] S. Barzegar-Parizi, M. R. Tavakol, and A. Khavasi, "Deriving surface impedance for 2-D arrays of graphene patches using a variational method," *IEEE J. Quantum Electron.*, vol. 53, no. 1, pp. 1–6, Feb. 2017.
- [20] T. K. Gaylord and M. G. Moharam, "Analysis and applications of optical diffraction by gratings," *Proc. IEEE*, vol. 73, no. 5, pp. 894–937, May 1985.
- [21] M. Shahabadi, S. Atakaramians, and N. Hojjat, "Transmission line formulation for the full-wave analysis of two-dimensional dielectric photonic crystals," *IEE Proc.-Sci., Meas. Technol.*, vol. 151, no. 5, pp. 327–334, Sep. 2004.
- [22] T. Tamir and S. Zhang, "Modal transmission-line theory of multilayered grating structures," *J. Lightw. Technol.*, vol. 14, no. 5, pp. 914–927, May 1996.
- [23] L. Li, "Use of Fourier series in the analysis of discontinuous periodic structures," *J. Opt. Soc. Amer. A, Opt. Image Sci.*, vol. 13, no. 9, pp. 1870–1876, Sep. 1996.
- [24] S. Khorasani and B. Rashidian, "Guided light propagation in dielectric slab waveguide with conducting interfaces," *J. Opt. A, Pure Appl. Opt.*, vol. 3, no. 5, p. 380, 2001.
- [25] S. Khorasani and B. Rashidian, "Modified transfer matrix method for conducting interfaces," *J. Opt. A, Pure Appl. Opt.*, vol. 4, no. 3, p. 251, 2002.
- [26] K. Mehrany, S. Khorasani, and B. Rashidian, "Novel optical devices based on surface wave excitation at conducting interfaces," *Semicond. Sci. Technol.*, vol. 18, no. 6, p. 582, 2003.
- [27] L. Ju *et al.*, "Graphene plasmonics for tunable terahertz metamaterials," *Nature Nanotechnol.*, vol. 6, no. 10, pp. 630–634, Sep. 2011.
- [28] Z. Fang *et al.*, "Gated tunability and hybridization of localized plasmons in nanostructured graphene," *ACS Nano*, vol. 7, no. 3, pp. 2388–2395, 2013.
- [29] L. Li, "New formulation of the Fourier modal method for crossed surface-relief gratings," *J. Opt. Soc. Amer. A, Opt. Image Sci.*, vol. 14, no. 10, pp. 2758–2767, 1997.
- [30] J. Hu, H. Zeng, C. Wang, Z. Li, C. Kan, and Y. Liu, "Interband  $\pi$  plasmon of graphene: Strong small-size and field-enhancement effects," *Phys. Chem. Chem. Phys.*, vol. 16, no. 42, pp. 23483–23491, 2014.
- [31] B. Fotouhi, V. Ahmadi, M. Abasifard, and R. Roohi, "Interband  $\pi$  plasmon of graphene nanopores: A potential sensing mechanism for dna nucleotides," *J. Phys. Chem. C*, vol. 120, no. 25, pp. 13693–13700, 2016.
- [32] F. H. L. Koppens, D. E. Chang, and F. J. G. de Abajo, "Graphene plasmonics: A platform for strong light-matter interactions," *Nano Lett.*, vol. 11, no. 8, pp. 3370–3377, Jul. 2011.
- [33] E. D. Palik, *Handbook of Optical Constants of Solids*, vol. 3. San Diego, CA, USA: Academic, 1998.
- [34] G. W. Hanson, "Dyadic Green's functions and guided surface waves for a surface conductivity model of graphene," *J. Appl. Phys.*, vol. 103, no. 6, p. 064302, 2008.
- [35] R. A. Jishi, M. S. Dresselhaus, and G. Dresselhaus, "Electron-phonon coupling and the electrical conductivity of fullerene nanotubes," *Phys. Rev. B, Condens. Matter*, vol. 48, pp. 11385–11389, Oct. 1993.

- [36] S. M. Raeis-Zadeh and S. Safavi-Naeini, "Application of graphene nanoholes as a terahertz polarizer," in *Proc. IEEE Int. Symp. Antennas Propag. USNC/URSI Nat. Radio Sci. Meeting*, Jul. 2015, pp. 1640–1641.
- [37] C. W. Berry and M. Jarrahi, "Broadband terahertz polarizing beam splitter on a polymer substrate," *J. Infr., Millim. Terahertz Waves*, vol. 33, no. 2, pp. 127–130, 2012.
- [38] M. Xu, H. P. Urbach, D. K. G. de Boer, and H. J. Cornelissen, "Wire-grid diffraction gratings used as polarizing beam splitter for visible light and applied in liquid crystal on silicon," *Opt. Exp.*, vol. 13, no. 7, pp. 2303–2320, Apr. 2005.

**Hoda Fadakar** received the B.S. and M.S. degrees in electrical engineering from the Isfahan University of Technology, Isfahan, Iran, in 2007 and 2009, respectively, where she is currently pursuing the Ph.D. degree. Her research interests include the diffraction analysis of periodic structures, plasmonic devices, nanophotonics, and theoretical and numerical methods in electromagnetics.



**Amir Borji** received the B.Sc. and M.Sc. degrees in electrical engineering from the Isfahan University of Technology, Isfahan, Iran, in 1994 and 1998, respectively, and the Ph.D. degree in electrical engineering from the University of Waterloo, Waterloo, ON, Canada, in 2004. He was with the Department of Electrical and Computer Engineering, University of Waterloo, as a Post-Doctoral Fellow from 2004 to 2006. From 2006 to 2012, he was with the Department of Electrical and Computer Engineering, Isfahan University of Technology, as an Assistant Professor. In 2012, he joined the Department of Electrical Engineering, Sharif University of Technology, Tehran, Iran, where he is currently an Assistant Professor. Since 2016, he has been with the Department of Electrical and Computer Engineering, University of Waterloo, as a Research Assistant Professor, where he is conducting research on the novel configurations of phased array antennas and millimeter-wave low-loss waveguide technologies.



**Abolghasem Zeidaabadi Nezhad** was born in Sirjan, Iran, in 1961. He received the B.Sc. degree in electronics engineering from the Shahid Bahonar University of Kerman, in 1988, and the M.Sc. and Ph.D. degrees in communication engineering from the Sharif University of Technology in 1991 and 1997, respectively. Since 1997, he has been with the Isfahan University of Technology, where he is currently an Associate Professor with the Department of Electrical and Computer Engineering. His areas of interest include antenna and microwave engineering.



**Mahmoud Shahabadi** received the B.Sc. and M.Sc. degrees from the University of Tehran, Tehran, Iran, in 1988 and 1991, respectively, and the Ph.D. degree from the Technische Universitaet Hamburg, Hamburg, Germany, in 1998, all in electrical engineering. Since 1998, he has been with the School of Electrical and Computer Engineering, University of Tehran, where he is currently a Full Professor and the Director of the Photonics Research Laboratory. From 2001 to 2004, he was a Visiting Professor with the Department of Electrical and Computer Engineering, University of Waterloo, Canada. His current research interests and activities encompass various areas of microwave, millimeter wave, and terahertz engineering, as well as photonics and plasmonics.